Modelling the structural behaviour of frost-damaged reinforced concrete structures

Modeling the Structural Behavior of Frost-damaged Reinforced Concrete Structures

Kamyab Zandi Hanjari[*a], Per Kettil[b], Karin Lundgren[a]

[a]*Department of Civil and Environmental Engineering, Chalmers University of Technology, Göteborg, Sweden*

[b]*Department of Applied Mechanics, Chalmers University of Technology, Göteborg, Sweden*

[*] Corresponding author's Email: kamyab.zandi@chalmers.se
Postal address: Chalmers University of Technology, SE – 412 96 Göteborg, Sweden

A methodology is introduced to predict the mechanical behavior of reinforced concrete structures with an observed amount of frost damage at a given time. It is proposed that the effects of internal frost damage and surface scaling can be modeled as changes of material and bond properties, and geometry, respectively. These effects were studied and suggestions were made to relate the compressive strength and dynamic modulus of elasticity, as the indicators of damage, to the response of the damaged concrete in compression and tension, and to the bond behavior. The methodology was applied to concrete beams affected by internal frost damage, using non-linear finite element analyses. A comparison of the results with available experimental data indicated that the changes in failure mode and, to a rather large extent, the effect on failure load caused by internal frost damage can be predicted. However, an uncertainty was the extension and distribution of the damaged region which affected the prediction of the load capacity.

Keywords: concrete structures; assessment; deterioration; damage; structural analysis

1. Introduction

There is a growing need for reliable methods to assess deteriorated concrete structures. Optimized maintenance and repair strategies require the capability to predict the load-carrying capacity and remaining service life of the damaged structures. The most severe types of deterioration in concrete structures are associated with the volume expansion of reinforcing bars and concrete, e.g. reinforcement corrosion and frost damage, respectively. This paper deals with the load-carrying capacity of frost-damaged reinforced concrete structures, which is still an evolving research topic in the assessment of existing structures.

Frost damage in concrete is caused by a) the differing thermal expansion of ice and concrete and b) by the volume expansion of freezing water in the concrete pore system (Chatterji 1999b). The former mechanism is involved when the structure is subjected to cold climates in the presence of saline water. The stress arises from the

difference in thermal expansion of ice and concrete, which leaves the ice in tension as the temperature drops. Therefore, a crack in brine ice penetrates into the substrate and causes the superficial damage known as surface scaling (Valenza and Scherer 2006). This damage usually results in spalling of the concrete surface, while the remaining concrete is mostly unaffected (Wiberg 1993, Gudmundsson and O. Wallevik 1999, Fagerlund 2004). The latter mechanism is involved when the volume expansion of the freezing water, restrained by the surrounding concrete, cannot be accommodated in the pore system. Thereby, tensile stresses are initiated and micro and macro cracks are introduced into the concrete body, which leads to the type of severe damage known as internal frost damage. This mechanism affects the compressive strength, tensile strength, elastic modulus, fracture energy, and the bond between the reinforcing bar and surrounding concrete in damaged regions (Powers 1945, Shih *et al.* 1988, Fagerlund *et al.* 2001).

While previous research has been primarily concerned with the causes and mechanisms of frost deterioration, relatively little attention has been given to the problem of assessing the load-carrying capacity of the damaged structures. A number of studies have investigated the mechanisms of frost damage (Beaudoin and MacInnis 1974, Chatterji 1999a, Valenza and Scherer 2006) and numerically modeled the effects of freezing and thawing on porous solids in a material level (Zuber and Marchand 2000, Kruschwitz and Bluhm 2005). Another group of experimental studies focused on the influence of frost on material properties of concrete (Fagerlund 2004, Hasan *et al.* 2004, Shang and Song 2006, Hasan *et al.* 2008) and the steel-concrete bond (Shih *et al.* 1988, Fagerlund *et al.* 1994, Petersen and Lohaus 2004). A few studies have been devoted to the structural response of frost-damaged concrete structures, including panels and slabs (Mohamed *et al.* 2000, Tang and Petersson 2004) and beams (Hassanzadeh and Fagerlund 2006, Petersen *et al.* 2007).

In an experimental study carried out by Hassanzadeh and Fagerlund (2006), bending tests were conducted on reinforced concrete beams subjected to freezing and thawing cycles. It was concluded that when the concrete is severely damaged, it may cause dramatic reductions of the load capacity and the stiffness of the structure, and may change the mode of failure. The structural response of frost-damaged beams in terms of moment-curvature relation has also been experimentally and numerically investigated by Petersen *et al.* (2007) and the freezing-and-thawing-induced change in tension stiffening has been discussed.

It should be noted that most of the previous numerical and analytical studies have focused on the mechanical behavior of frost-damaged structures in service limit state. The aim of this paper is to devise a method to quantify the damage caused by freezing of reinforced concrete, in terms of the mechanical behavior and load-carrying capacity of the structure in ultimate limit state. First, a methodology to analyze the mechanical behavior of frost-damaged concrete structures, as changes in the effective material and bond properties and geometry of a damaged concrete member, is proposed. Second, a short summary of the beam tests carried out by Hassanzadeh and Fagerlund (2006) is presented; these beams are the basis for comparison with the finite element (FE) analysis. Finally, the experimental and numerical results are compared and the application of the proposed procedure to actual structures is discussed.

2. Methodology to Analyze the Mechanical Behavior of Frost-damaged Concrete Structures

A methodology to analyze the mechanical behavior and to determine the remaining load-carrying capacity of reinforced concrete structures affected by frost damage is presented. The methodology is based on the premise that the effect of internal frost damage can be modeled as changes in material and bond properties. Moreover, the effect of surface scaling can be taken into account as a change in geometry, such as a reduction in concrete cross-section when surface scaling leads to cover spalling while the remaining concrete is assumed to be unaffected (Wiberg 1993). The methodology is restricted to the prediction of the mechanical behavior of a structure with an observed amount of damage at a given time; hence, the formation of the damage over time is not included.

In the assessment of the damaged structures, the compressive strength and the dynamic modulus of elasticity, as indicators of damage, must be measured in each individual case. The compressive strength can be evaluated by compression tests on a few drilled cores, supplemented with non-destructive tests to determine the extent of the damaged region. The dynamic modulus of elasticity can be evaluated using either ultrasonic transit time measurement or fundamental transverse frequency test. Frost damage changes the internal structure of concrete, by introducing micro and macro cracks, which lengthens the travel time of an ultrasonic wave through the damaged concrete. It is believed that there is a strong correlation between the level of frost damage and the dynamic modulus of elasticity (Petersen *et al.* 2007, Zandi Hanjari *et al.* 2009b, Zandi Hanjari *et al.* 2009a). Such a correlation can be suggested using the available test data in the literature; see Figure 1. Thereafter, the effect of frost damage on material properties, such as the stress-strain response in compression, the stress-crack opening relation in tension and the bond-slip behavior, is estimated using the damage indicators. Finally, the behavior of the damaged structure can be studied in the finite element (FE) analysis. Within this context, suggestions are given on how the effect of frost can be taken into account as changes in the effective material and bond properties. Reference is made to several tests performed and models developed by other authors, in order to clarify different aspects of the methodology.

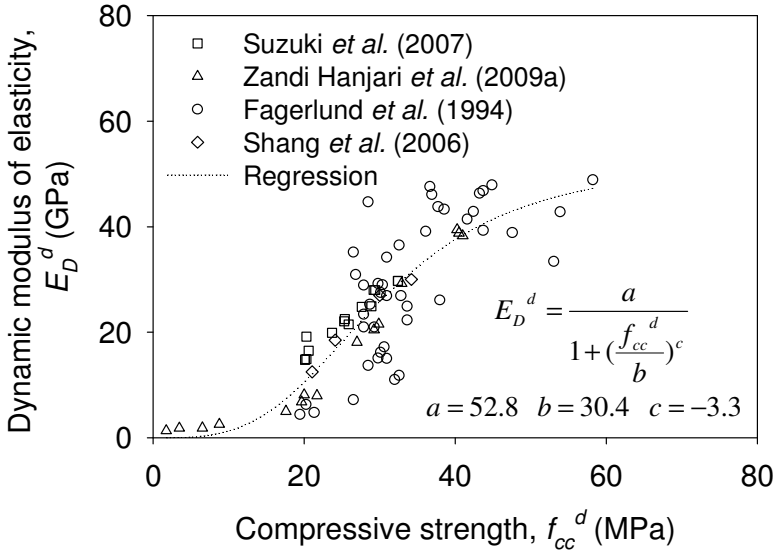

Figure 1. Correlation between compressive strength and dynamic modulus of elasticity for frost-damaged concrete.

2.1. Relation between Compressive and Tensile Strength

For undamaged concrete, the relation between compressive strength and tensile strength is well-established and widely used; e.g. see CEB-FIP Model Code 1990 (1993) and EuroCode 2. For practical reasons, to reduce the number of tests required to compression tests only, it would be useful if similar relations could be found for frost-damaged concrete. Test results for the tensile strength of undamaged and frost-damaged concrete were adapted and plotted versus the corresponding compressive strength and compared with relations for undamaged concrete, Figure 2(a). In the study carried out by Fagerlund *et al.* (1994), specimens have been cast from eleven concrete batches with different water/cement ratios of 0.5, 0.65 and 0.8. The pre-dried specimens have been evacuated to different residual pressures of 2, 20 and 50 mmHg. Then water has been introduced in the vacuum chamber and the specimens have been reached different degrees of saturation. Finally the specimens have been exposed to seven freeze-thaw cycles, each cycle with a duration of two days and a minimum temperature of -18˚C. The higher the degree of vacuum was, the higher the degree of saturation and the more severe damage was reached.

In Figure 2(a), the compressive strength was recalculated from a dry 100 mm cube to a 150 mm cube by multiplying it by 0.96 (Neville 1996), and then to the standard wet 150 × 300 mm cylinder which is commonly used in codes by multiplying it by 0.85 (CEB-FIP 1993). The tensile strength was obtained from the measured splitting tensile strength by multiplying it by 0.9. As can be seen, the relations for the undamaged concrete cannot be used directly for the frost-damaged concrete. The tensile strength of the damaged concrete is markedly lower than if it was estimated from the relations for undamaged concrete. By curve fitting, although the scatter is large, the following relation for the damaged concrete is found:

$$f_{ct}{}^{d} = 0.027 \cdot \left(f_{cc}{}^{d}\right)^{1.2} \qquad (1)$$

where $f_{ct}{}^{d}$ is the tensile strength of the damaged concrete, and $f_{cc}{}^{d}$ is the measured compressive strength of the damaged concrete in MPa using a standard 150 × 300 mm cylinder.

Subsequently, the proposed relationship was compared with experimental work carried out by other researchers (Hassanzadeh and Fagerlund 2006, Shang and Song 2006, Zandi Hanjari *et al.* 2009a). It should be noted that the proposed relation is independent of environmental conditions and only considers the observed amount of damage, i.e. compressive strength of the damaged concrete, at a given time. As shown in Figure 2(b), the tensile strength of the damaged concrete was reasonably well estimated by Equation (1), and the deviation from experimental results remained less than 18%.

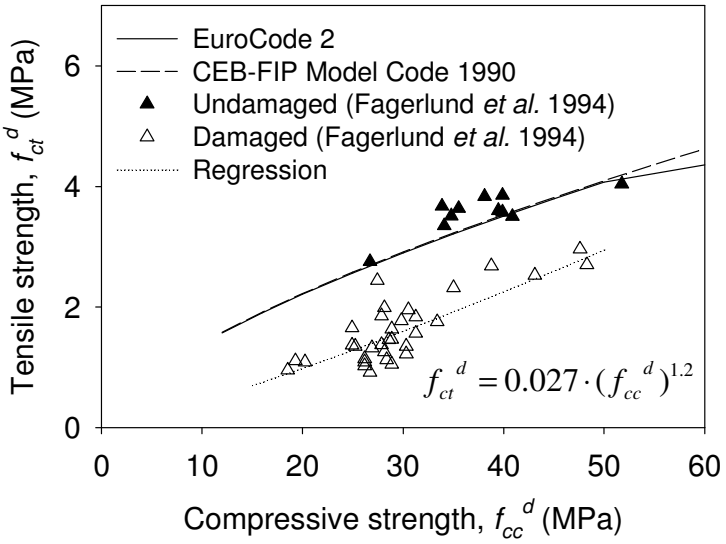

(a)

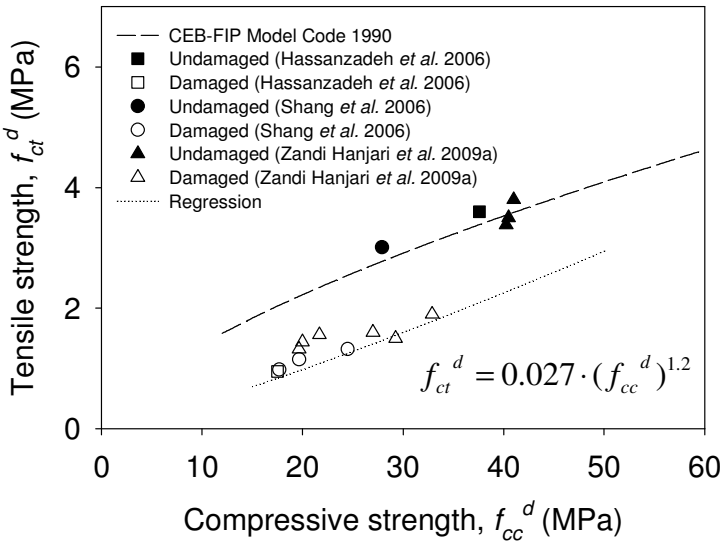

(b)

Figure 2. Compressive strength versus tensile strength of frost-damaged concrete from (a) Fagerlund *et al.* (1994) and (b) other experimental investigations.

2.2. Behavior in Compression

The cracks caused by the internal frost damage influence the response of the concrete in compression (Suzuki and Ohtsu 2004). The damaged concrete exhibits a considerably lower initial elastic modulus, a relatively larger strain at the peak stress and a more ductile response in the post-peak behavior compared to the undamaged concrete (Shang and Song 2006, Hasan *et al.* 2008). In an earlier work, concrete

cylinders with two levels of frost damage corresponding to approximately 25 and 50% reduction in compressive strength were tested in compression (Zandi Hanjari *et al.* 2009a). It was observed that the ascending branch of the stress-strain relation is subjected to a change of the stiffness. This is believed to be caused by the randomly oriented cracks in the concrete due to the damage before the specimens were subjected to loading. Consequently, loading starts on a concrete specimen of low stiffness before the cracks are closed, and then the loading continues with a stiffer concrete (Ueda *et al.* 2009). However, the stiffness never fully recovers and a permanent stiffness loss is observed (Zandi Hanjari *et al.* 2009a). These effects are here taken into account by adapting the stress-strain relation of the undamaged concrete according to a model by Thorenfeldt *et al.* (1987) to make it work for the damaged concrete.

$$\sigma_{cc} = f_{cc}^{\,d}\left(\frac{\varepsilon}{\varepsilon_{cc}^{\,d}}\right)\cdot\left(\frac{n}{n-1+\left(\frac{\varepsilon}{\varepsilon_{cc}^{\,d}}\right)^{n\cdot k}}\right) \tag{2}$$

where σ_{cc} and ε are the stress and strain in the concrete, respectively, and $\varepsilon_{cc}{}^{d}$ is the strain at the maximum stress. The correction factors, n and k, are calculated as follows:

$$n = \frac{E_c^{\,d}}{E_c^{\,d} - E_0^{\,d}} \tag{3}$$

$$k = \begin{cases} 1 & \text{for} \quad 0 < \varepsilon < \varepsilon_{cc}^{\,d} \\ 0.67 + \dfrac{f_{cc}^{\,d}}{62} & \text{for} \quad \varepsilon > \varepsilon_{cc}^{\,d} \end{cases} \tag{4}$$

where $E_c{}^{d}$ and $E_0{}^{d}$ are the secant and tangential elastic modulus of the damaged concrete, respectively. The strain at the maximum stress, $\varepsilon_{cc}{}^{d}$, can be estimated by means of the experimental data, Figure 3(a), and the secant elastic modulus is calculated as $f_{cc}{}^{d}/\ \varepsilon_{cc}{}^{d}$. An approximation of the tangential elastic modulus of the damaged concrete based on the dynamic modulus of elasticity has been given by Petersen (2003); see Figure 3(b). Relatively good agreement is seen when the approximation is compared with the later experimental data (Suzuki *et al.* 2007, Zandi Hanjari *et al.* 2009a). The analytical stress-strain response of the damaged concrete from Equation (2) is compared with that of the experimental data from Zandi Hanjari *et al.* (2009a) in Figure 4.

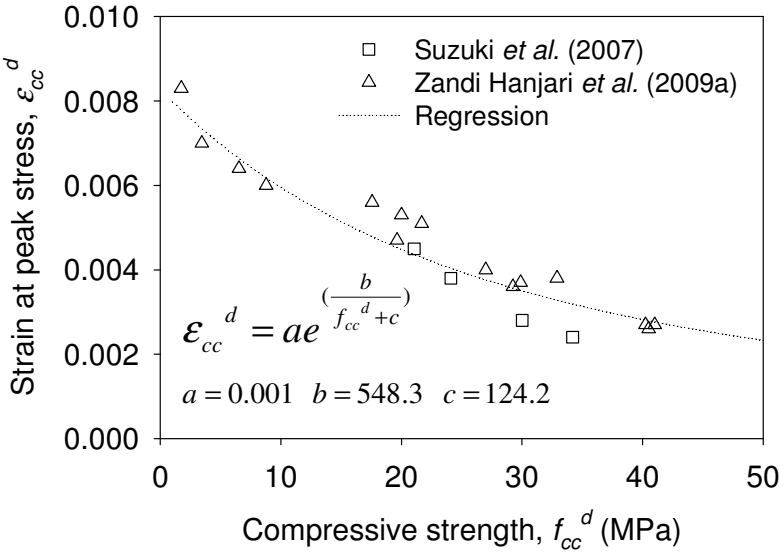

(a)

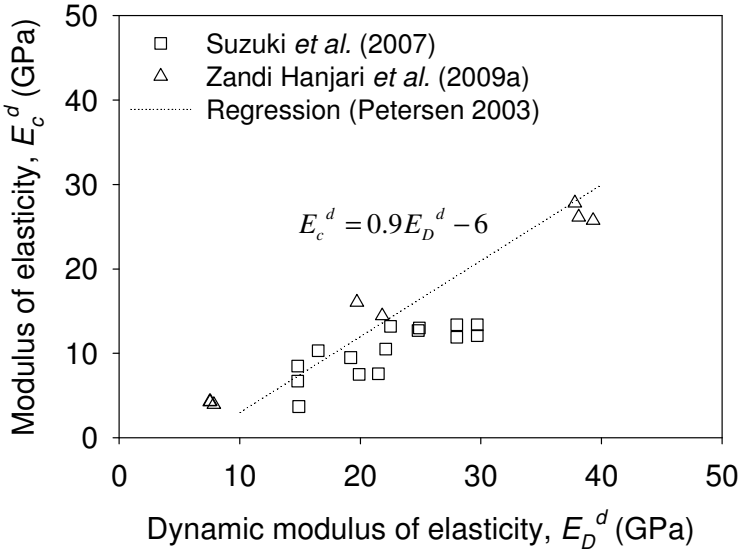

(b)

Figure 3. Estimation of the (a) strain at peak stress and (b) tangential elastic modulus for the damaged concrete, using the damage indicators, $f_{cc}{}^{d}$ and $E_D{}^{d}$.

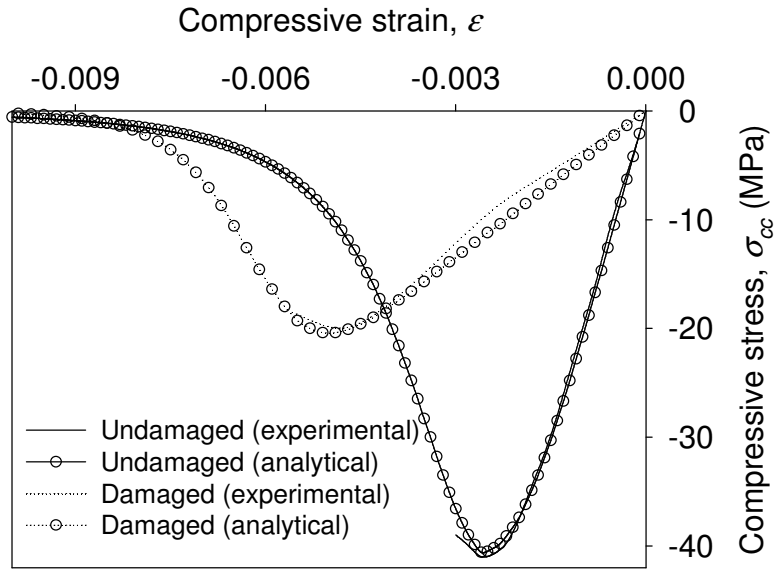

Figure 4. Stress-strain response in compression; the level of frost-damage corresponds to 50% reduction in compressive strength (Zandi Hanjari et al. 2009a).

2.3. Behavior in Tension

The tensile strength of the frost-damaged concrete has been investigated using splitting tensile tests (Fagerlund *et al.* 1994, Shang and Song 2006, Zandi Hanjari *et al.* 2009a) and wedge splitting tests (Zandi Hanjari *et al.* 2009a). A slightly larger effect of frost damage on the tensile strength than on the compressive strength has been reported; see Figure 1. However, there is very little information concerning the softening behavior of the frost-damaged concrete. This is particularly important because of the direct application of such a relation in numerical analyses. In a recent study (Zandi Hanjari *et al.* 2009a), a bi-linear relation between tensile stress, σ_{ct}, and crack opening, w, of the frost-damaged concrete was estimated by using inverse analysis carried out on wedge splitting test results. The test were performed on cylinder specimens of 100 × 100 mm, damaged to two levels equivalent to 25 and 50% reduction in compressive strength, damage levels I and II in Figure 5(a).

It was found that the fracture energy and the critical crack opening, corresponding to zero tensile stress, significantly increased by the evolution of damage. Relatively large increase in fracture energy, up to approximately 170 Nm/m^2, was also reported by other researchers (Hassanzadeh and Fagerlund 2006); see Figure 5(b). To the best of knowledge of the authors, the bi-linear σ_{ct}-w relation given by Zandi Hanjari *et al.* (2009a) is the only data available in the literature which can be used as input in finite element analysis of frost-damaged concrete; see Figure 5(a).

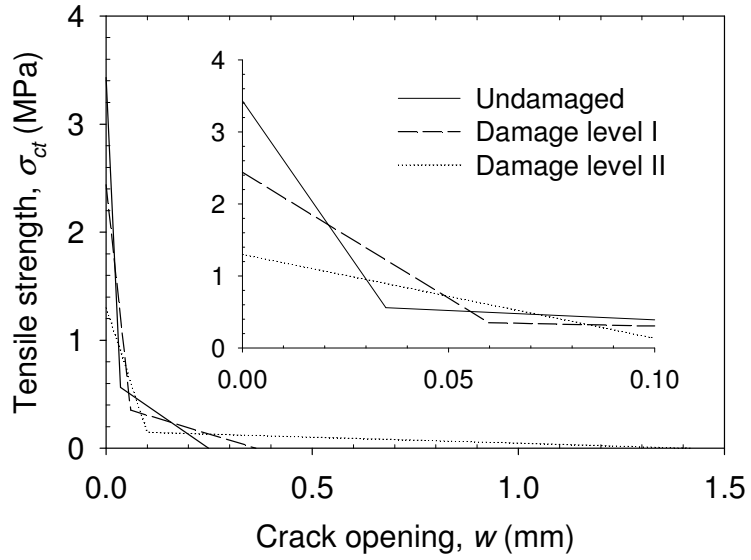

(a)

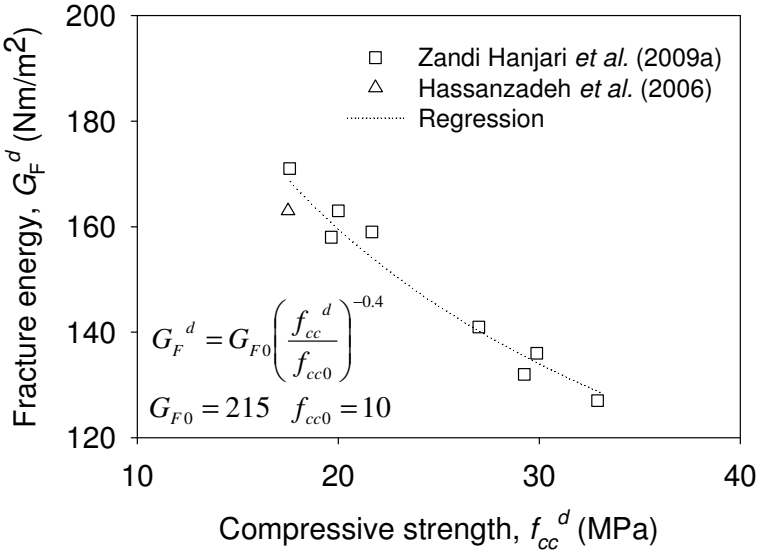

(b)

Figure 5. (a) Bi-linear σct-w relation; damage levels I and II correspond to 25 and 50% reduction in compressive strength (Zandi Hanjari et al. 2009a); (b) the effect of frost damage on fracture energy.

2.4 Bond Behavior

Available experimental studies concerning the effect of frost damage on the bond between the reinforcement and concrete lead to the following three conclusions:

- In spite of a large scatter, the tests show an obvious influence of frost on the bond strength. Fagerlund *et al.* (1994) suggested lower and upper bound

values for the reduction of the bond strength equal to 30 and 70%. Zandi Hanjari *et al.* (2009b) reported 15 and 50% bond deterioration for frost damage levels equivalent to 25 and 50% reduction in compressive strength. A linear decrease of the bond strength with the increase of damage was suggested by other researchers (Petersen *et al.* 2007, Ji *et al.* 2008).

- For a low level of damage, when the effect of frost is limited to the concrete cover, a small decrease of the slip at the maximum bond stress is observed (Petersen *et al.* 2007). For a large damage, when the effect of frost is extended to the interface between the concrete and the reinforcement, the bond capacity suddenly decreases and the slip slowly increases (Shih *et al.* 1988, Petersen *et al.* 2007, Zandi Hanjari *et al.* 2009b).
- The residual bond strength, represented by a constant stress after the descending branch of the bond stress-slip relationship, decreases with increased damage level (Zandi Hanjari *et al.* 2009b).

The bond stress-slip relation proposed by CEB-FIB Model Code 90 (1993) is here modified to incorporate frost effects. In regions where the concrete cover has totally spalled off due to surface scaling, the bond strength is assumed to be zero. In other areas where the cover still remains (but may be cracked), the bond-slip properties are estimated based on the following approximations:

1) The relation between bond strength, τ_b, and slip, s, given in CEB-FIB Model Code 90 (1993) are adopted for the undamaged concrete. To account for intermediate cases in between the extreme cases "confined" (i.e. ductile pull-out failure) and "unconfined" (i.e. brittle failure due to cover cracking induced by the radial tensile stress), the following interpolation formula was proposed by Lundgren *et al.* (2009):

$$\tau_b = k_{\text{int}} \cdot \tau_{b,confined} + (1 - k_{\text{int}}) \cdot \tau_{b,unconfined} \tag{5}$$

The interpolation factor is determined by

$$k_{\text{int}} = \max \begin{cases} k_{c/\phi} \\ k_{Asw} \end{cases} \tag{6}$$

where $k_{c/\phi}$ is a factor that depends on the ratio of cover to bar diameter, c/ϕ; k_{Asw} is a factor that depends on the amount of effective shear reinforcement, A_{sw}/s_w; and s_w is the shear reinforcement spacing. Factors $k_{c/\phi}$ and k_{Asw} are chosen according to Figure 6.

2) The variation of the maximum bond stress in relation with the frost damage quantified with the relative dynamic modulus of elasticity was formulated by Petersen *et al.* (2007):

$$\tau_{\max}{}^{d} = \left(0.17 + 0.007 \cdot E_{D,rel}{}^{d}\right) \cdot \tau_{\max} \tag{7}$$

where $\tau_{\max}{}^{d}$ and $\tau_{\max}$ are the bond strength for damaged and undamaged concrete, respectively, and $E_{D,rel}{}^{d}$ is the relative dynamic modulus of elasticity for the damaged concrete.

3) The residual bond strength is reduced proportionally to the reduction in the bond capacity (Zandi Hanjari *et al.* 2009b).

$$\tau_f{}^{d} = \left(\frac{\tau_{\max}{}^{d}}{\tau_{\max}} \right) \cdot \tau_f \tag{8}$$

where $\tau_f{}^{d}$ and τ_f are the residual bond strength for damaged and undamaged concrete, respectively.

The analytical bond-slip relation for the damaged concrete, Equations (5)-(8), is compared with that of the experimental data from Zandi Hanjari *et al.* (2009b) in Figure 7.

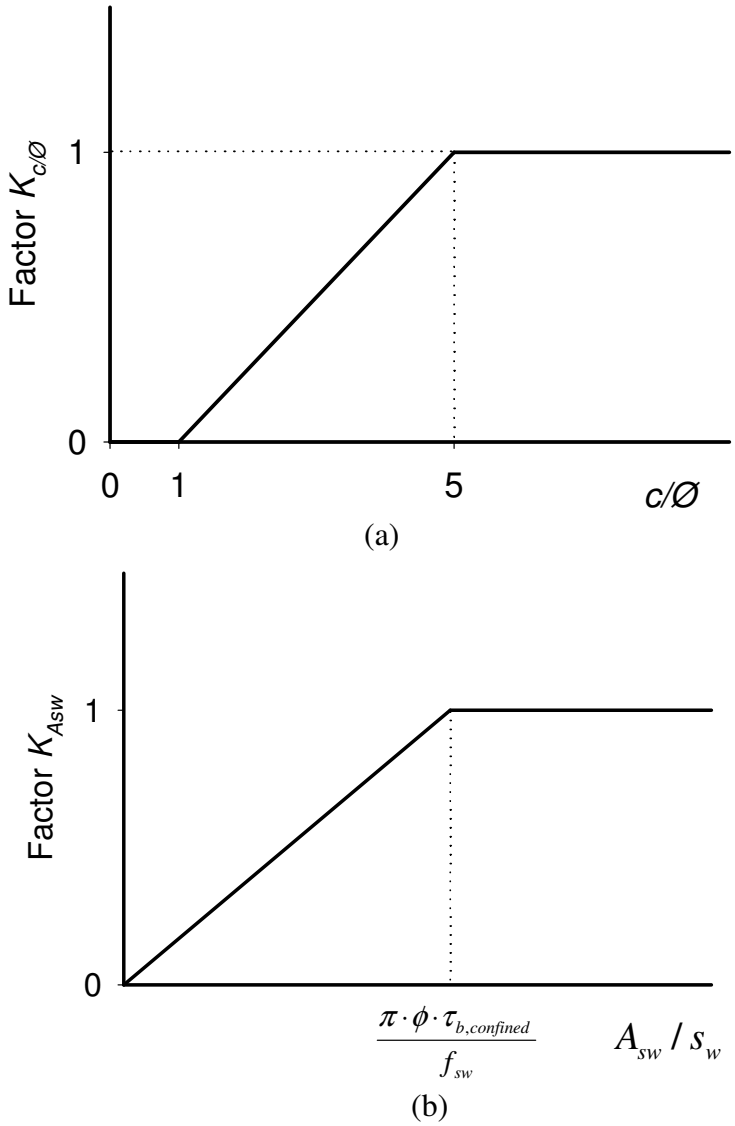

Figure 6. Interpolation factors (Lundgren et al. 2009).

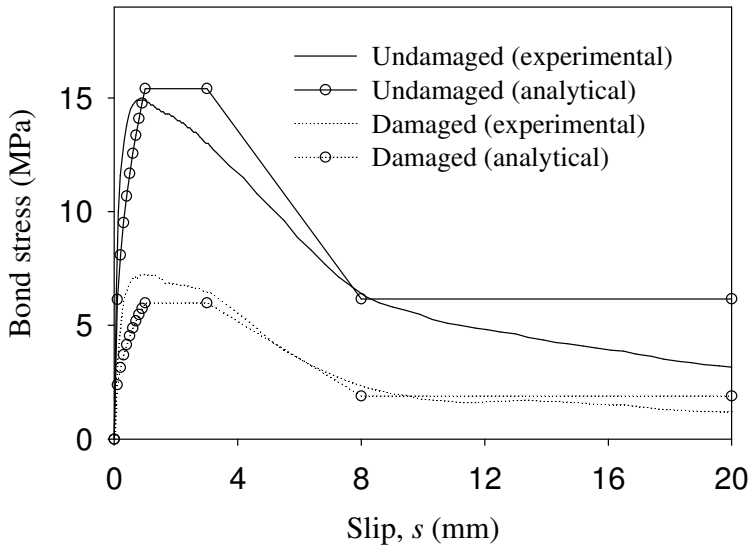

Figure 7. Bond-slip relation for "Good" bond condition; the level of frost-damage corresponds to 50% reduction in compressive strength (Zandi Hanjari et al. 2009b).

3. Frost-damaged Beam Tests for Comparison with FE Analysis

In an experimental program, Hassanzadeh and Fagerlund (2006) have studied the effect of frost damage on the load-carrying capacity of beams. Twelve beam tests were carried out including two geometries with varied reinforcement content and stirrups; see Table 1 and Figure 8. The reference beams were exposed to a laboratory climate. The other beams were vacuum treated to a residual pressure of 2 mmHg followed by submerging in water. Thereafter, they were subjected to two complete freeze-thaw cycles with a constant temperature at -21±1ºC inside a climate chamber. The compressive strength, splitting tensile strength and fracture energy of concrete have been measured; see Table 2. The splitting tensile strength of the concrete exposed to freezing has been determined for 80 × 80 mm cores drilled from concrete blocks of 1 × 0.4 × 0.2 m stored under the same conditions as the damaged beams. The specimens exposed to freezing showed typical internal frost damage with no sign of surface scaling.

Varying amount of longitudinal reinforcement and stirrups, combined with two concrete cross-sections, led to a different behavior of the beams in both service and ultimate limit states. The frost damage reduced the strength and elastic modulus of the concrete, which changed the stiffness of the beams in service limit state. To better understand the behavior of the beams in ultimate limit state, the conditions for brittle and ductile bending failures were investigated analytically for all reference and damaged beams; see Table 3. It is seen that, the frost effect reduced the compressive strength of the concrete as well as the bond capacity, so that all of the damaged beams showed brittle failure.

Table 1. Beam types (Hassanzadeh and Fagerlund 2006).

Type	*l* *[m]*	*h* × *b* *[mm]*	*d* *[mm]*	*Tensile reinforcement*	*Stirrup*	*ρ* *[%]*	*Beam names*	
							Reference	*Damaged*
1	4.4	500 × 200	430	4Ø20	28Ø8	1.46	R1	D1
2	3.0	300 × 200	260	3Ø20	18Ø8	1.81	R2	D2
3	4.4	500 × 200	430	6Ø20	32Ø8	2.19	R3	D3
4	3.0	300 × 200	230	5Ø20	22Ø8	3.41	R4	D4
5	4.4	500 × 200	430	4Ø20	8Ø8	1.46	R5	D5
6	3.0	300 × 200	260	3Ø20	8Ø8	1.81	R6	D6

Note: *l* is length of the beams; *h* and *b* are height and width of the cross-sections; *d* is the effective height; and *ρ* is reinforcement ratio (A_s/bd).

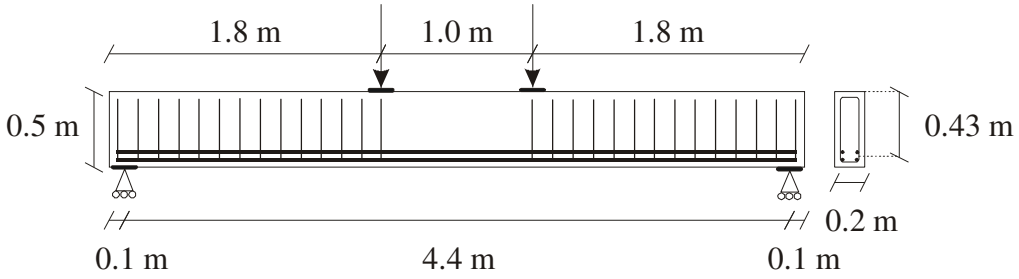

(a)

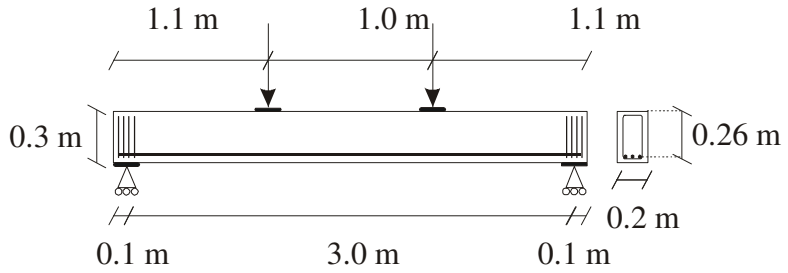

(b)

Figure 8. Examples of the beam: (a) type 1 and (b) type 6 (Hassanzadeh and Fagerlund, 2006).

Table 2. Properties of concrete (Hassanzadeh and Fagerlund 2006).

Properties		*Test method*	*Beam condition*	
			Undamaged	*Frost-damaged*
Compressive strength	[MPa]	Cylinder 100 × 200 mm	37.6	17.50
Splitting tensile strength	[MPa]	Cylinder 100 × 200 mm	4.1	0.95
Fracture energy	[N/m]	Three-point-bending test (RILEM)	139.0	163.0

Note: compressive and splitting tensile strength of the frost-damaged concrete were determined from tests on 80 × 80 mm concrete cores; the strength values has been multiplied by 0.85 to be comparable with the strength of undamaged concrete (Hassanzadeh and Fagerlund 2006).

Table 3. Analytically predicted failure mode of the studied beams.

Type	*d*	*b*	A_s	ρ	*Undamaged beams*		*Frost-damaged beams*	
	[mm]	*[mm]*	*[mm²]*	*[%]*	ρ/ρ_b	*Failure*	ρ/ρ_b	*Failure*
1	430	200	1256	1.46	0.84	Ductile	1.72	Brittle
2	260	200	942	1.81	1.05	Balance	2.13	Brittle
3	430	200	1884	2.19	1.27	Brittle	2.58	Brittle
4	230	200	1570	3.41	1.97	Brittle	4.02	Brittle
5	430	200	1256	1.46	0.84	Ductile	1.72	Brittle
6	260	200	942	1.81	1.05	Balance	2.13	Brittle

Note: ρ_b is balanced reinforcement ratio and A_s is tensile reinforcement content.

4. Finite Element Analysis

The load-carrying capacity of all reference and frost-damaged beams, tested by Hassanzadeh and Fagerlund (2006), was calculated with 2D finite element analysis according to the proposed methodology. The beams were modeled using plane stress elements and the interaction between the longitudinal reinforcement and the concrete was modeled with a bond-slip mechanism; however, the stirrups were embedded in the plane stress concrete elements by assuming full interaction.

4.1. FE Model and Numerical Procedure

Due to geometrical symmetry and with the assumption of symmetry in the damaged zone around the middle of the beam, only half of the beam was included in the model; see Figure 9. In the tests, steel plates and roller bearings have been used at the supports. In the FE model, the steel plate was modeled as infinitely stiff by constraint equations. The FE nodes along the plate were tied to the centre node, thus forcing the nodes to remain in a straight line, but allowing for rotation. The centre node was supported for displacement in the *y*-direction. For modeling of the loading plates on the top of the beam, the nodes were also tied to remain in a straight line. At the symmetry line, all the nodes were fixed in the *x*-direction.

An incremental static analysis was made using an explicitly specified load step size and a Newton-Raphson iterative scheme to solve the non-linear equilibrium equations. In a phased analysis, the self-weight load was first applied. Thereafter, the beam was subjected to the external load as a prescribed displacement at the loading point.

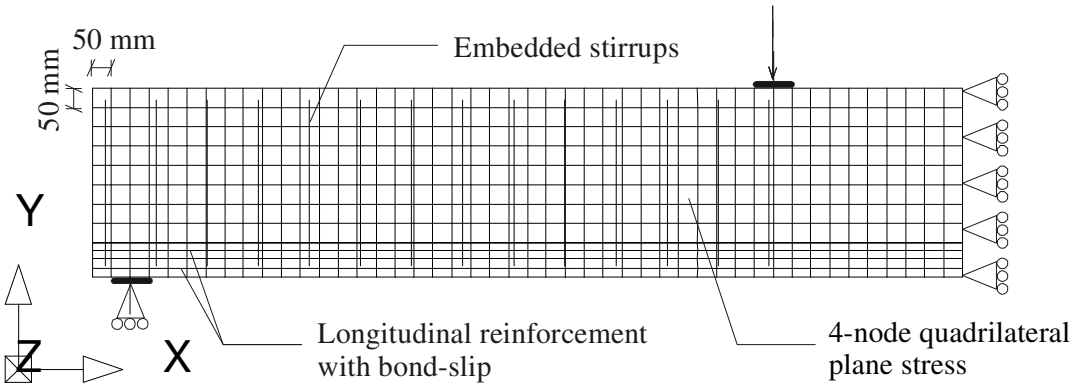

Figure 9. Finite element model of the studied beams.

4.2. Modeling of the Concrete

For the concrete, four-node quadrilateral plane stress solid elements were used. The concrete was modeled with a constitutive model based on non-linear fracture mechanics using a smeared rotating crack model based on total strain (DIANA 2009). The crack band width was assumed to be equal to the element size, 50 mm. This was later verified to be a good approximation of the localization zone.

In the analysis of the reference beams, the behavior of concrete in tension was taken into account according to the model by Hordijk (1991). For the frost-damaged beams, the bi-linear tensile stress-crack opening relation, given by Zandi Hanjari *et al.* (2009a), for a damaged concrete with 50% reduction in compressive strength was used. This was an acceptable assumption as the reported compressive strength of the damaged beams indicated approximately 53% reduction compared with that of the reference beams; see Table 2.

For the behavior of concrete in compression, the stress-strain curve according to Thorenfeldt *et al.* (1987) was used for the reference beams. The same relation was adapted according to the proposed methodology and used in the analysis of the damaged beams. When the stress-strain relationship is used in numerical analyses, localization of the deformations in compressive failure needs to be taken into account. The compression softening behavior is related to the boundary conditions and the size of the specimen (Mier 1984). Consequently, as the stress-strain relation by Thorenfeldt *et al.* (1987) has been calibrated by measurements of compression tests on 300 mm long cylinders, the softening branch needs to be modified for the concrete element size used in the FE model, Figure 10. This was done by assuming that the compressive failure would take place in one element row. This assumption was later found to be correct in the analysis. The main difficulty with this method of compression behavior modeling is that the number of elements in which the compressive region will localize is not known in advance. While in tension, it seems reasonable to assume that a crack will localize in one element row.

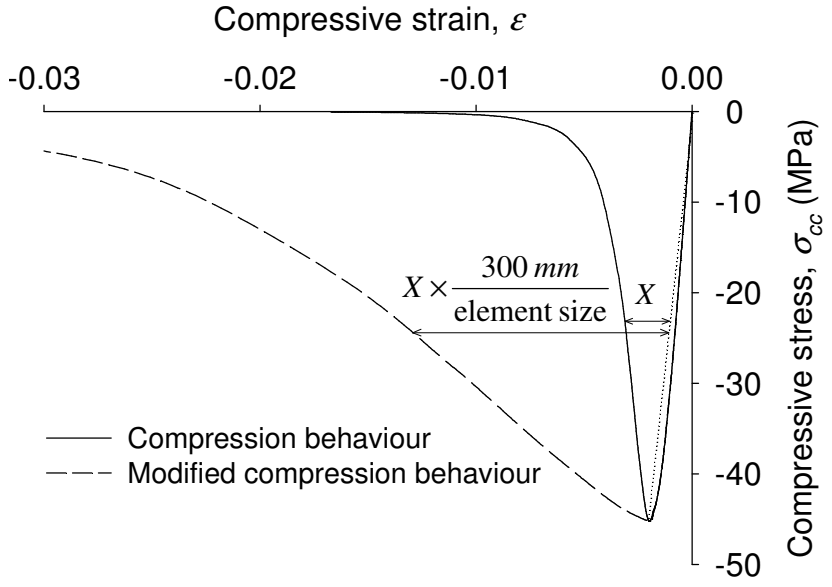

Figure 10. Modification of the stress-strain relation with respect to the concrete element size in the FE model.

4.3. Modeling of Reinforcement and Concrete-Reinforcement Interaction

The longitudinal reinforcement was modeled by two-node truss elements. Interaction between the reinforcement and the concrete was modeled with a bond-slip relation. Interface elements, describing the bond-slip behavior in terms of a relation between the tractions and the relative displacements, were used across the reinforcement and the concrete interface. The analytical bond-slip relation for confined concrete under "Good" bond conditions given in the CEB-FIP Model Code (1990) was assumed for the reference beams. The same relation was adapted according to the proposed modifications and used in the analysis of the damaged beams. The stirrups were embedded in the concrete elements, corresponding to a perfect bond between the stirrups and concrete. The embedded stirrups add stiffness to the concrete elements; their strain is calculated from the displacement field of the plane stress elements (DIANA 2009).

Since the reinforcement type used in the experiments was not reported by Hassanzadeh and Fagerlund (2006), the reinforcement steel was modeled in the finite element analyses as elastic ideal-plastic; the yield stress was calibrated so that the maximum load agreed with the experimental result for the reference beam R1. The same yield stress, 670 MPa, and elastic modulus, 200 GPa, were used for the rest of the analyses.

5. Results of the FE Analysis

With respect to the design rules for reinforced concrete beams at the ultimate limit state, the failure mode of an undamaged beam depends on the reinforcement ratio, in such a way that a lightly reinforced beam is expected to fail in bending due to yielding of reinforcement, while a heavily reinforced beam is excepted to fail in bending due to concrete crushing. A moderately reinforced beam may fail in either of the modes. A flexural member is also subjected to shear stresses which may lead to diagonal cracks. Unless a properly detailed cross-section and appropriate amount of transverse and longitudinal reinforcements are provided, diagonal cracks may results in shear failure. Other failure modes may also govern the behavior of a beam; however, the beams in the experimental program of Hassanzadeh and Fagerlund (2006) were designed to fail in one of the described modes.

In this context, the behavior of the reference and damaged beams is studied in the following. The results from the numerical analyses and experiments are presented and compared in three groups with respect to the cross-section and the governing failure mode of the beams. The load versus midspan deflection of the beams from the experiments and the numerical analyses are presented in Figures 11-13. The crack distributions in terms of principal tensile strains from the analyses are shown in Figures 14 and 15.

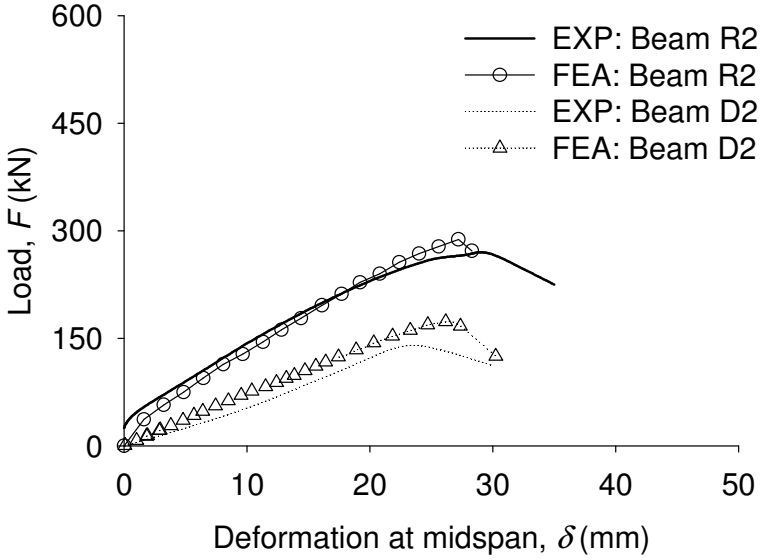

(a)

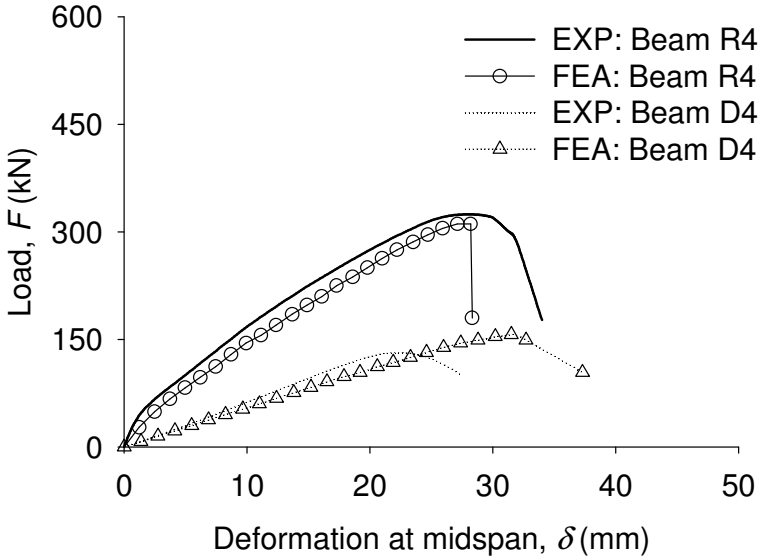

(b)

Figure 11. Load-deformation for beams (a) type 2 and (b) type 4.

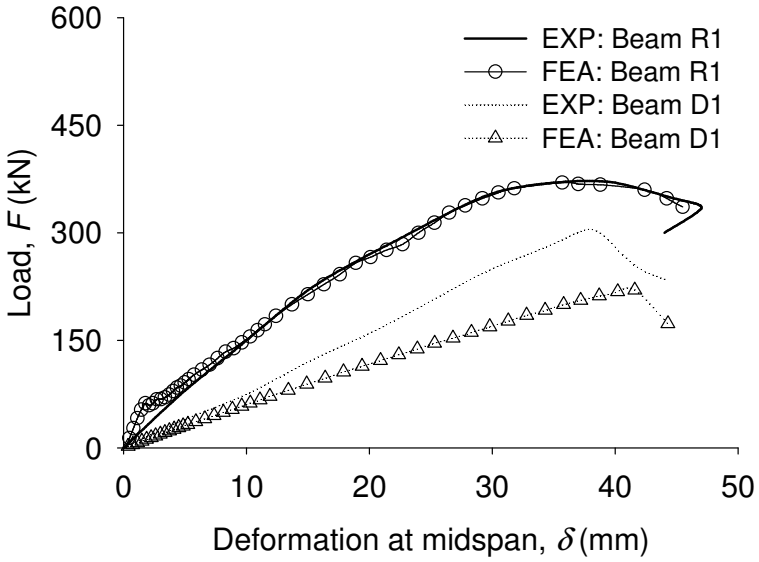

(a)

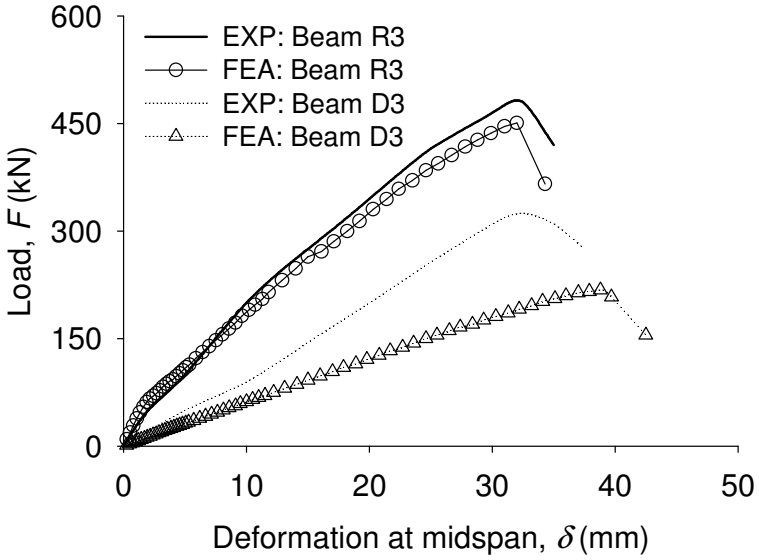

(b)

Figure 12. Load-deformation for beams (a) type 1 and (b) type 3.

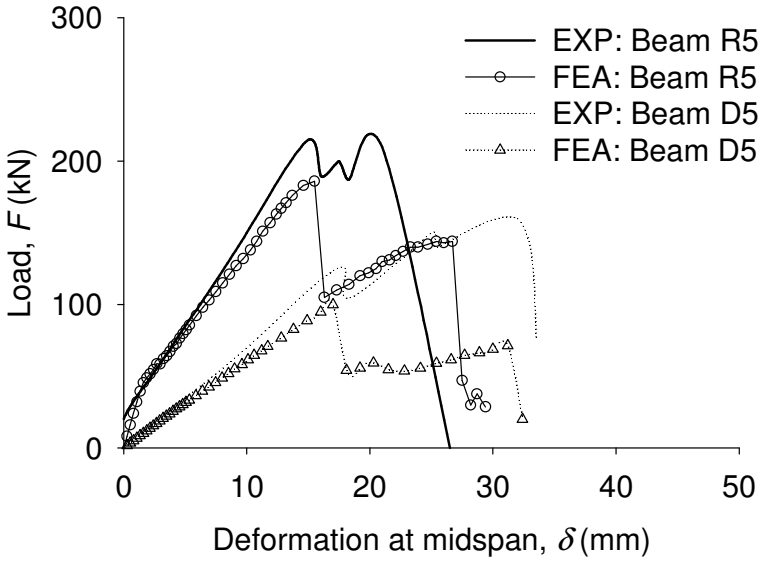

(a)

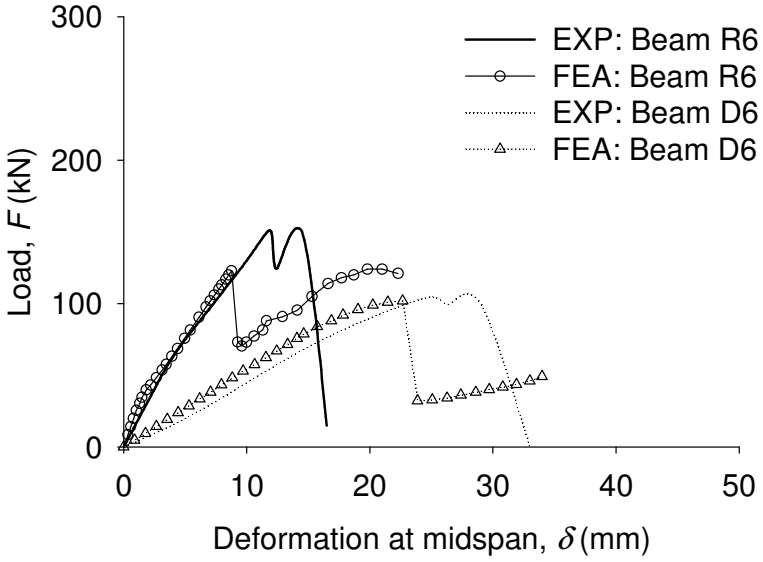

(b)

Figure 13. Load-deformation for beams (a) type 5 and (b) type 6.

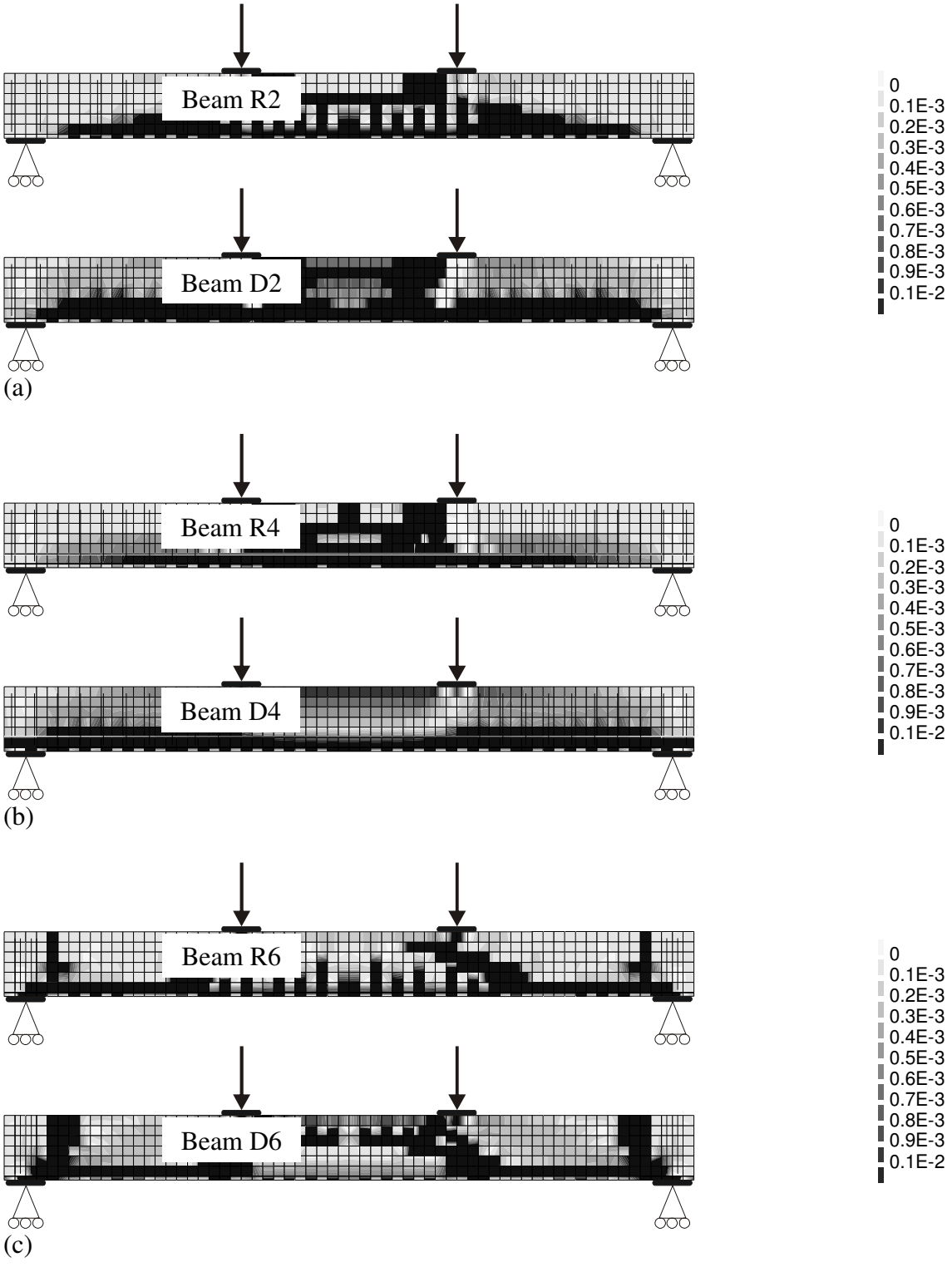

Figure 14. Crack pattern in terms of the maximum tensile strains from numerical analyses of beams (a) type 2, (b) type 4 and (c) type 6.

5.1. Beams with Smaller Cross-section and Bending Failure: Types 2 and 4

According to Table 3, the beam type 2 had tightly spaced stirrups and was moderately reinforced in the tension zone, meaning that the reference beam was expected to fail in bending either due to yielding of reinforcement or crushing of concrete. Numerical analysis has shown that the reference beam R2 failed due to concrete crushing in compression zone shortly after the tensile reinforcement yielded which corresponded to a progressive loss of ductility. This agrees with the observations from the experiment, Figure 11(a). Due to extensive deterioration of concrete, the failure of the damaged beam D2 was only governed by crushing of concrete in the compression zone. The stiffness reduction and the load and deformation at the failure were estimated quite well by the numerical analysis. The crack pattern from the analysis of the reference beam showed bending cracking for a very low load level followed by an initiation of shear cracking before the concrete crushing took place, Figure 14(a). In the analysis of the damaged beam, progressive longitudinal cracking along the tensile reinforcement occurred prior to crushing of concrete. However, the capacity of both beams, R2 and D2, were limited by crushing of concrete.

Due to high bending reinforcement content and presence of shear reinforcement, the reference beam R4 failed in a brittle manner as a result of concrete crushing without prior yielding of the reinforcement, both in the test and the analysis, Figure 11(b). The load capacity of the damaged beam D4 in the test was limited by concrete crushing at the upper edge of the beam, similar to the reference one. In the analysis, relatively high compressive stresses were appeared in the compressive zone, but the lack of anchorage capacity over the supports was the primary failure mode of the damaged beam, Figure 14(b). From the experimental observations, the extension of the freezing-induced cracks for this beam were perpendicular to the direction of the longitudinal axis of the beam; while in the other damaged beams, the extension of the cracks was mostly parallel to the direction of the beam's longitudinal axis (Hassanzadeh and Fagerlund 2006). The direction of the cracks has decisive influence on the fracture of concrete in compression. Delamination of concrete due to compressive stress is facilitated when the extension of cracks has the same direction as the compressive stresses. However, this effect is not taken into account in the numerical modeling. That was the reason for the disagreement seen between the experiment and the analysis of the damaged beam D4.

5.2. Beams with Larger Cross-section and Bending Failure: Types 1 and 3

Beam type 1 had tightly spaced shear reinforcement and was lightly reinforced in the tension zone. Therefore, a rather ductile bending failure of the reference beam R1 due to yielding of the reinforcement was expected. This failure mode was observed both in the experiment and in the numerical analysis, Figures 12(a) and 15(a). In the analysis, yielding of the reinforcement was followed by compressive failure of the concrete at a relatively large midspan deflection.

For the damaged beam D1, extensive deterioration of concrete led to the crushing of concrete in the compression zone prior to yielding of reinforcement. This agrees with the failure mode observed in the experiments. However, the analysis underestimated the failure load and the stiffness of the damaged beam. This is believed to be due to unevenly distribution of frost damage in the large beams. Hassanzadeh and Fagerlund (2006) have visually observed that the beams with larger

cross-section were severely damaged at the surface, but less damaged at the inner part. However, the level of damage has been quantified in terms of compressive strength and splitting tensile strength of 80 × 80 mm cores drilled out from frost-damaged blocks of 1 × 0.4 × 0.2 m. As the blocks had smaller dimensions than the large beams, the level of damage measured from the blocks can be expected to be higher than that of the large beams. Furthermore, the length of the cores was 80 mm whereas the height of the beam was 500 mm. Although the material properties were tested on cores drilled out from different locations in the block and the average value was reported, the strength of the inner concrete, deeper than 80 mm, was not taken into account. Petersen *et al.* (2007) has shown that the distribution of frost damage may significantly differ at various distances from the exposed surface. Therefore, the material and bond properties used as input for the numerical analyses most likely corresponded better to the beams with smaller cross-section.

Due to high bending reinforcement content, the reference beam R3 failed in a brittle manner as a result of concrete crushing without prior yielding of the reinforcement in the test. The numerical analysis was able to predict the failure mode, initial stiffness, and load carrying-capacity of the reference beam quite well.

For the damaged beam D3, the analysis showed a bending failure due to crushing of concrete followed by an anchorage failure over the support. As explained before, the stress-strain relation of the damage concrete exhibits a rather large strain at peak stress. Therefore, the soft behavior of damaged concrete in the compression zone allows for large midspan deformation of the beam before any concrete crushing takes place. This explains why anchorage was observed as the secondary failure mode in the numerical analysis. Concrete crushing limited the load capacity of the damaged beam D3 in the experiments; no indication of any secondary failure mode was reported by Hassanzadeh and Fagerlund (2006). The same argument made for the beam D1 is valid for this beam as well; i.e. the beams with larger cross-section were damaged less than the concrete blocks used for quantification of the damage. This explains the underestimation of the strength and stiffness and overestimation of the deformation at failure of the damaged beams D1 and D3.

5.3. Beams with Shear Failure; Types 5 and 6

The load versus the deformation of the reference beam R5 is plotted in Figure 13(a). The beam had the same cross-section and longitudinal reinforcement as the beam R1 but without distributed stirrups. Diagonal shear cracking limited the capacity of the beam in the test at a load of approximately 220 kN; this was estimated to be about 200 kN according to the provisions given in EuroCode 2. The numerical analysis estimated a failure load of approximately 190 kN and showed that inclined shear cracking governed the failure of the beam. The evolution of cracks in the analysis explains the two peak loads at about 190 and 140 kN observed in the analysis. In the analysis, Figure 14(c), a few bending cracks formed for a rather small load levels; this caused the change in the initial stiffness. For a larger load, shear cracks appeared and reached the tensile reinforcement in the middle of the shear span; this governed the failure of the beam and formed the first peak in the load-deformation curve. Thereafter, longitudinal cracks propagated along the reinforcement towards the end of the beam. These cracks stopped at the support regions where four closely spaced stirrups were placed. Finally, the formation of the vertical cracks next to the support resulted in an anchorage failure; this corresponds to the second peak in the load.

A rather large influence of frost was seen in the capacity of this beam, Figure 13(a). The beam D5 failed in shear, similar to the reference beam, at a load level of 125 kN. This was estimated to be approximately 150 kN according to EuroCode 2 using the damaged material properties. The analysis also showed a shear failure at a load of approximately 110 kN followed by an anchorage failure in the support region, Figure 15(c). The evolutions of diagonal and longitudinal cracks in the analysis were similar to that of the reference beam. The crack pattern from the numerical analysis showed that the diagonal cracks in the damaged beam formed with a greater angle to the longitudinal axis compared to the diagonal cracks in the reference beam. This is mainly because of the effect of frost on the compressive strength of concrete. As the compressive strength decreases, the shear stress required to cause cracking decreases and the inclination of the cracks to the longitudinal axis increases.

Beam type 6 had the same amount of shear reinforcement as the beam type 5 but with smaller cross-section. Therefore, larger effect of frost was expected on the capacity of beam type 6 as it was more damaged. For both the reference and the damaged beams, shear cracking limited the load capacity in the experiments and the analyses, Figures 13(a) and 14(c). Numerical analysis estimated the capacity of the damaged beam quite well.

In the analyses of the beams failed in shear, types 5 and 6, the results kept on the safe side. The load capacity and the deformation at the failure loads were slightly underestimated. This can be explained by two aspects of the analysis: a) the tension softening of concrete and b) the stiffness of longitudinal reinforcement in transverse direction. When concrete cracks, tensile stresses are transferred due to tension softening. In reinforced concrete, stresses are also transmitted across the crack by the bond action between the reinforcement and the concrete. In a situation where the crack is subjected to shear loading, additional stresses are transferred due to friction. Therefore, if tension softening of concrete is estimated when only fracture energy of concrete is taken into account, the results will keep on the safe side, (Broo *et al.* 2008), as it was in the analyses presented here. The second explanation concerns with the modeling of longitudinal reinforcement. When diagonal cracks form, the ability of concrete to transmit tensile stresses is severely reduced unless appropriate reinforcement is present. In reality, the reinforcement has stiffness parallel and perpendicular to the bar axis. However, the tensile reinforcement, modeled with truss elements in the FE analysis, had stiffness only along the bar axis. This contributes to underestimation of the results in the post-peak behavior.

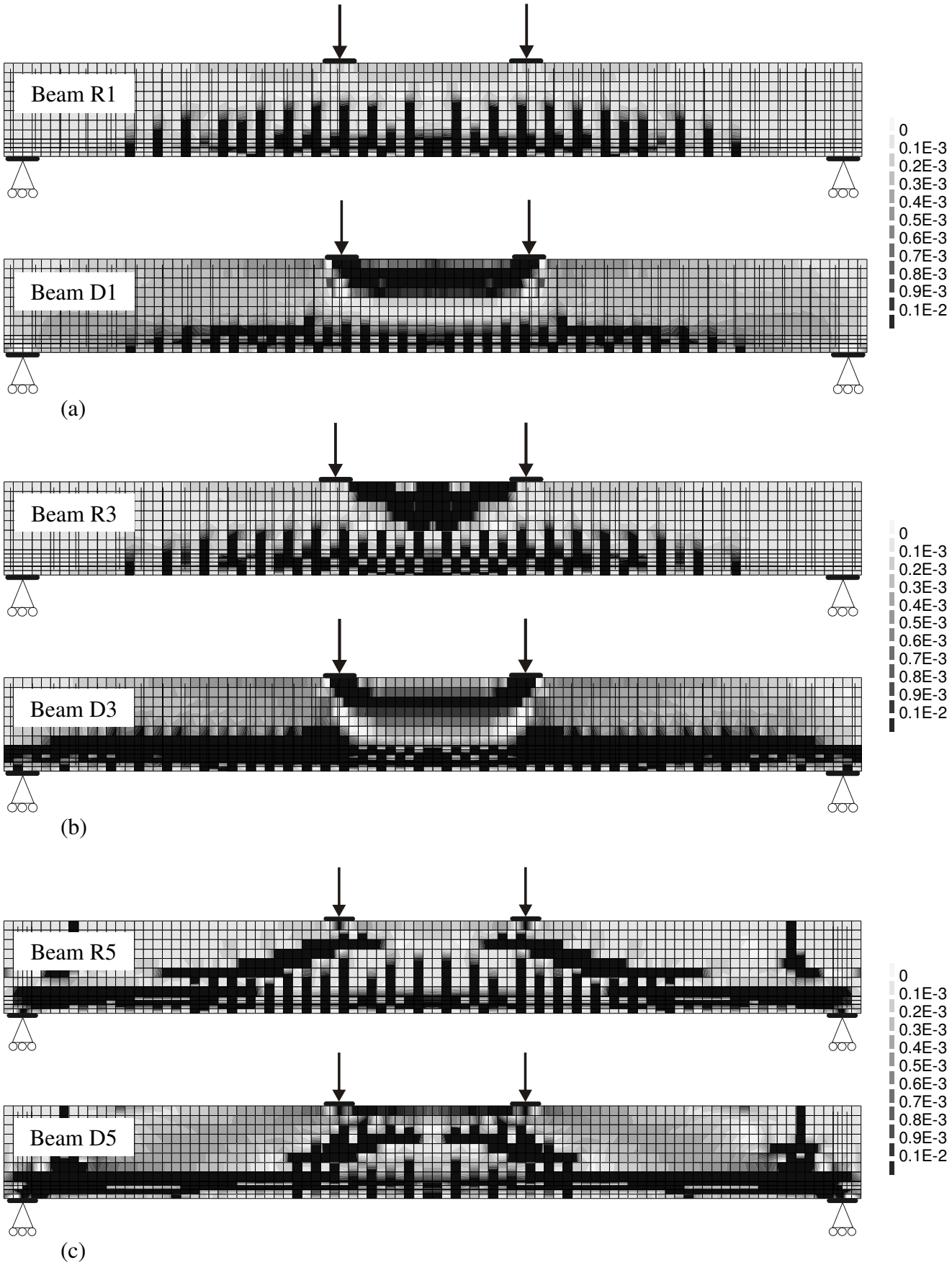

Figure 15. Crack pattern in terms of the maximum tensile strains from numerical analyses of beams (a) type 1, (b) type 3 and (c) type 5.

6. Summary of Results, Discussion and Application

The capability of the proposed methodology for evaluation of the remaining load-carrying capacity of the frost-damaged beams is illustrated in Figure 16. It is seen that the failure load and deformation at the peak load were better estimated for the reference beams than the damaged beams. The results from numerical analysis keep on the safe side except for the damaged beams D2 and D4; however, the overestimation in the failure load remained less than 25 %. This was partly due to the direction of the cracks which were along the axis of the beam and had decisive influence on the fracture of concrete in compression. Beams with larger cross-section, D1 and D3, were less damaged than the other beams. That has led to an underestimation of the failure load in the analysis. For the beams with shear failure, D5 and D6, an underestimation of the failure load was seen. This was expected as the tension softening of concrete was determined when only fracture energy of concrete was taken into account; the favorable effects of bond action and friction across the shear crack were disregarded.

The experimental and numerical results showed a large stiffness deterioration in the load-displacement response of all the damaged beams. Such a stiffness loss was seen both before and after bending cracks. An explanation of the loss of the stiffness in pre-peak behavior of the damaged beams can be found in the chain of events: considerable reduction of the concrete elastic modulus, relatively softer behavior of concrete in tension after cracking and partial bond deterioration leading to the loss of tension stiffening. Some analyses carried out by the authors showed that the elastic modulus of concrete has the largest influence on the stiffness. Reduction in elastic modulus of frost-damaged concrete may be as high as 85% (Zandi Hanjari *et al.* 2009a).

The evolution of cracks in the analysis of the beams with shear failure showed that diagonal cracks in a frost-damaged beam form with a greater angle to the longitudinal axis of the beam compared to that in an undamaged beam. This is believed to be due to the effect of frost on the compressive strength of concrete.

In the assessment of deteriorated structures, hand calculation and numerical analysis at different levels can be done following the methodology presented in this paper. Hand calculations may be sufficient for assessing the bending capacity, while the ductility can only be captured by use of a numerical model, including bond-slip behavior. Furthermore, numerical modeling can be carried out at different levels: structural, component or detail levels. At the structural level, a whole structure can be modeled using simplified linear structural analysis with beam and/or shell elements. Simple modeling and reduced analysis time are the two advantages of structural analysis. This allows to change the model easily and to handle more alternatives. Some analyses at the structural level carried out by the authors gave satisfactory results when the capacity of the damaged beam was limited by a bending failure; these analyses are not presented here. More complex failure modes, such as shear and anchorage, require more detailed modeling of the bond-slip behavior and shear reinforcement. At the component level, similar to the analysis presented in this paper, non-linear analysis using solid elements can be carried out. The effects of damage can be included by modification of the concrete cross-section, the response of the materials in tension and compression, and the bond-slip relation. At the detail level, the deterioration and disintegration of the material can be analyzed at the microstructure level.

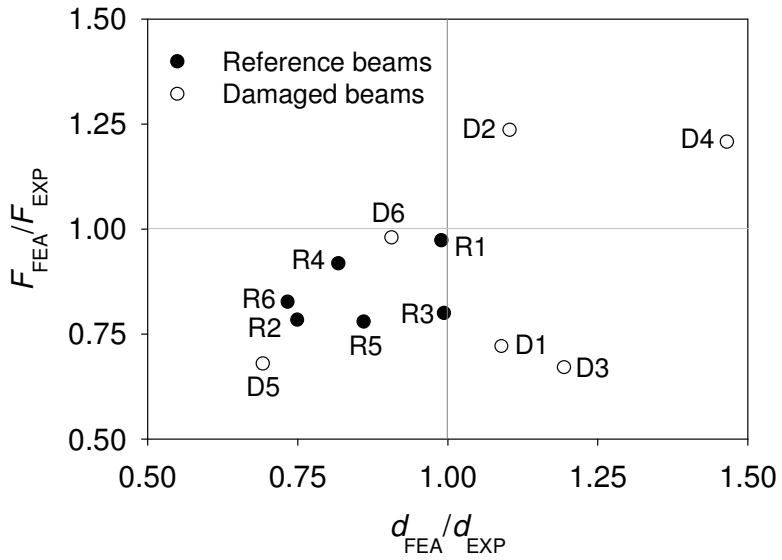

Figure 16. Comparison of results from experiments and numerical analyses in terms of maximum load and deformation at the peak load.

7. Conclusions

A methodology to analyze the mechanical behavior of reinforced concrete structures affected by frost damage was introduced. It was proposed that the effects of internal frost damage and surface scaling can be modeled as changes in the material and bond properties as well as the cross-section of the damaged concrete member. First, the change in material and bond properties was established by using previous research. Then, the proposed methodology was tested on concrete beams affected by internal frost damage. The results of the analyses were compared with the available beam tests (Hassanzadeh and Fagerlund 2006). Based on this study the following conclusions are drawn.

1) Frost damage has a significant influence on the behavior of concrete in compression and tension. The bond between the reinforcement and the concrete is considerably affected by frost. All these together may change the behavior of a reinforced concrete member subjected to freezing.
2) These effects are suggested to be taken into account by relating the compressive strength and dynamic modulus of elasticity, as the indicators of damage, to the material response of a damaged concrete.
3) The change in material properties due to the effect of frost may lead to a change in the failure mode and more brittle behavior of a structure at failure. A comparison of the results with available experimental data indicated that the changes in failure mode and, to a rather large extent, the effect on failure load caused by internal frost damage can be predicted by using the proposed methodology.
4) An uncertainty was the extension and distribution of the damaged region over the cross-section which affected the prediction of the failure load and deformation.

Notation

A_s tensile reinforcement content

A_{sw} area of shear reinforcement

$E_c^{\ d}$ secant elastic modulus of damaged concrete

$E_0^{\ d}$ tangential elastic modulus of damaged concrete

$E_D^{\ d}$ dynamic modulus of elasticity for damaged concrete

$E_{D,rel}^{\ d}$ relative dynamic modulus of elasticity for damaged concrete

F load

G_F fracture energy of undamaged concrete

$G_F^{\ d}$ fracture energy of damaged concrete

b width of concrete cross-section

c concrete cover

d, h effective height and height of concrete cross-section

f_{cc} compressive strength of undamaged concrete

$f_{cc}^{\ d}$ compressive strength of damaged concrete

f_{ct} tensile strength of undamaged concrete

$f_{ct}^{\ d}$ tensile strength of damaged concrete

f_{sw} yield strength of shear reinforcement

k_{int} interpolation factor

$k_{c/\phi}$ factor that depends on the ratio of cover to bar diameter

k_{Asw} factor that depends on the amount of effective shear reinforcement

k, n correction factors

s slip

s_w shear reinforcement spacing

w crack opening

δ deformation

ε compressive strain in concrete

$\varepsilon_{cc}^{\ d}$ compressive strain at the maximum stress for damaged concrete

$\rho; \rho_b$ reinforcement ratio; balanced reinforcement ratio

ϕ bar diameter

σ_{cc} compressive stress in concrete

σ_{ct} tensile stress in concrete

$\tau; \tau_b$ bond stress; bond strength

$\tau_{b,confined}$ bond strength for “confined” concrete

$\tau_{b,unconfined}$ bond strength for “unconfined” concrete

$\tau_{\max}$ maximum bond strength for undamaged concrete, model parameter

$\tau_{\max}^{\ d}$ maximum bond strength for damaged concrete, model parameter

τ_f residual bond strength for undamaged concrete, model parameter

$\tau_f^{\ d}$ residual bond strength for damaged concrete, model parameter

References

Beaudoin, J.J. and Macinnis, C., 1974. The mechanism of frost damage in hardened cement paste. Cement and Concrete Research, 4 (2), 139–147.

Broo, H., Lundgren, K. and Plos, M., 2008. A guide to non-linear finite element modelling of shear and torsion in concrete bridges. Report 2008:18, Civil and Environmental Engineering, Chalmers University of Technology, Göteborg, Sweden.

CEB-FIP, 1993. CEB-FIP model code 1990. Lausanne, Switzerland: Bulletin d'Information 213/214.

Chatterji, S., 1999a. Aspects of freezing process in porous material-water system Part 2. Freezing and properties of frozen porous materials. Cement and Concrete Research, 29 (5), 781–784.

Chatterji, S., 1999b. Aspects of the freezing process in a porous material-water system Part 1. Freezing and the properties of water and ice. Cement and Concrete Research, 29 (4), 627–630.

Diana finite element analysis, 2009. User's Manual - release 9.3. TNO Building and Construction Research, Delft, Netherlands.

ENV1992-1-1, 2004. Eurocode 2: Design of concrete structures - part 1: General rules and rules for buildings. CEN European Committee for Standardization, Brussels, 225.

Fagerlund, G., 2004. A service life model for internal frost damage in concrete. Report TVBM-3119, Lund Institute of Technology, Sweden.

Fagerlund, G., Janz, M. and Johannesson, B., 1994. Effect of frost damage on the bond between reinforcement and concrete. Report, Division of Building Materials, Lund Institute of Technology, Sweden.

Fagerlund, G., Somerville, G. and Jeppson, J., 2001. Manual for assessing concrete structures affected by frost. Division of Building Materials, Lund Institute of Technology, Sweden.

Gudmundsson, G. and Wallevik, O., 1999. Concrete in an aggressive environment. In: J. Janssen, M.J. Setzer, M.B. Snyder, ed. International RILEM Workshop on Frost Damage in Concrete, Proceeding 25, 28-30 June 1999 Minneapolis, USA: RILEM Publications S.A.R.L, 87–102.

Hasan, M., Okuyama, H., Sato, Y. and Ueda, T., 2004. Stress-strain model of concrete damaged by freezing and thawing cycles. Journal of Advanced Concrete Technology, 2 (1), 89–99.

Hasan, M., Ueda, T. and Sato, Y., 2008. Stress-strain relationship of frost-damaged concrete subjected to fatigue loading. Journal of Materials in Civil Engineering, 20 (1), 37–45.

Hassanzadeh, M. and Fagerlund, G., 2006. Residual strength of the frost-damaged reinforced concrete beamsed. In: C.A. Mota Soares, ed. III European Conference on Computational Mechanics Solids, Structures and Coupled Problems in Engineering, 5–8 June 2006 Lisbon, Portugal.

Hordijk, D.A., 1991. Local approach to fatigue of concrete. Thesis (PhD). Delft University of Technology.

Ji, X., Song, Y. and Liu, Y., 2008. Effect of freeze-thaw cycles on bond strength between steel bars and concrete. Journal Wuhan University of Technology, Materials Science Edition, 23 (4), 584–588.

Kruschwitz, J. and Bluhm, J., 2005. Modeling of ice formation in porous solids with regard to the description of frost damage. Computational Materials Science, 32 (3-4), 407–417.

Lundgren, K., Kettil, P., Zandi Hanjari, K., Schlune, H. and San Roman, A.S., 2009. Analytical model for the bond-slip behaviour of corroded ribbed reinforcement. Structure and Infrastructure Engineering, DOI: 10.1080/15732470903446993.

Mier, van J.G.M (Jan), 1984. Strain-softening of concrete under multiaxial loading conditions. Thesis (PhD). Eindhoven University of Technology.

Neville, A.M., 1996. Properties of concrete. London: John Wiley & Sons.

Mohamed, O.A., Rens, K.L. and Stalnaker, J.J., 2000. Factors affecting resistance of concrete to freezing and thawing damage. Journal of Materials in Civil Engineering, 12 (1), 26–32.

Petersen, L., 2003. Einfluss baustofflicher schädigungsprozesse auf das tragverhalten von stahlbetonbauteilen. Thesis (PhD). Universität Hannover.

Petersen, L. and Lohaus, L., 2004. Influence of chemical and physical loads on deteriorational design studies - concrete properties, bond and bending behaviored. 2nd Internation Conference Lifetime Oriented Design Concepts, Bochum, Germany.

Petersen, L., Lohaus, L. and Polak, M.A., 2007. Influence of freezing-and-thawing damage on behavior of reinforced concrete elements. ACI Materials Journal, 104 (4), 369–378.

Powers, T.C., 1945. A working hypothesis for further studies of frost resistance of concrete. Journal of American Concrete Institute, 16 (4), 245–271.

Shang, H.S. and Song, Y.P., 2006. Experimental study of strength and deformation of plain concrete under biaxial compression after freezing and thawing cycles. Cement and Concrete Research, 36 (10), 1857–1864.

Shih, T.S., Lee, G.C. and Chang, K.C., 1988. Effect of freezing cycles on bond strength of concrete. Journal of Structural Engineering, 114 (3), 717–726.

Suzuki, T. and Ohtsu, M., 2004. Quantitative damage evaluation of structural concrete by a compression test based on AE rate process analysis. Construction and Building Materials, 18 (3), 197–202.

Suzuki, T., Ohtsu, M. and Shigeishi, M., 2007. Relative damage evaluation of concrete in a road bridge by AE rate-process analysis. Materials and Structures, 40 (2), 221–227.

Tang, L. and Petersson, P.E., 2004. Slab test: Freeze/thaw resistance of concrete - internal deterioration. Materials and Structures, 37 (274), 754–759.

Thorenfeldt, E., Tomaszewicz, A. and Jensen, J.J., 1987. Mechanical properties of high-strength concrete and applications in designed. Conference on Utilization of High-Strength Concrete, Stavanger, Norway.

Ueda, T., Hasan, M., Nagai, K., Sato, Y. and Wang, L., 2009. Mesoscale simulation of influence of frost damage on mechanical properties of concrete. Journal of Materials in Civil Engineering, 21 (6), 244–252.

Valenza, J.J. and Scherer, G.W., 2006. Mechanism for salt scaling. Journal of the American Ceramic Society, 89 (4), 1161–1179.

Wiberg, U., 1993. Material characterization and defect detection in concrete by quantitative ultrasonics. Thesis (PhD). Kungl Tekniska Högskolan.

Zandi Hanjari, K., Utgenannt, P. and Lundgren, K., 2009a. Frost-damaged concrete: Part 1. Material properties. 4th International Conference on Construction

Materials: Performance, Innovations and Structural Implications. Nagoya, Japan, 753–760.

Zandi Hanjari, K., Utgenannt, P. and Lundgren, K., 2009b. Frost-damaged concrete: Part 2. Bond properties. 4th International Conference on Construction Materials: Performance, Innovations and Structural Implications. Nagoya, Japan, 761–766.

Zuber, B. and Marchand, J., 2000. Modeling the deterioration of hydrated cement systems exposed to frost action - part 1: Description of the mathematical model. Cement and Concrete Research, 30 (12), 1929–1939.